*Research Article*

# A Path Loss Model for Non-Line-of-Sight Ultraviolet Multiple Scattering Channels

## Haipeng Ding,[1] Zhengyuan Xu,[1] and Brian M. Sadler[2]

[1] *Department of Electrical Engineering, University of California, Riverside, CA 92521, USA*
[2] *Army Research Laboratory, RDRL-CIN, Adelphi, MD 20783, USA*

Correspondence should be addressed to Zhengyuan Xu, dxu@ee.ucr.edu

An ultraviolet (UV) signal transmission undergoes rich scattering and strong absorption by atmospheric particulates. We develop a path loss model for a Non-Line-of-Sight (NLOS) link. The model is built upon probability theory governing random migration of photons in free space, undergoing scattering, in terms of angular direction and distance. The model analytically captures the contributions of different scattering orders. Thus it relaxes the assumptions of single scattering theory and provides more realistic results. This allows us to assess the importance of high-order scattering, such as in a thick atmosphere environment, where short range NLOS UV communication is enhanced by hazy or foggy weather. By simulation, it is shown that the model coincides with a previously developed Monte Carlo model. Additional numerical examples are presented to demonstrate the effects of link geometry and atmospheric conditions. The results indicate the inherent tradeoffs in beamwidth, pointing angles, range, absorption, and scattering and so are valuable for NLOS communication system design.

## 1. Introduction

In free space optical communication, the deep ultraviolet (UV) spectrum with wavelength 200~280 nm is regarded as an appealing choice to overcome solar background radiation and relax pointing and tracking [3]. High altitude ozone absorbs most solar radiation in this band, yielding negligible background noise at sea level [4]. And, atmospheric scattering is very strong, enabling non-line-of-sight (NLOS) communications where the transmitter is not necessarily within the receiver field of view (FOV). However, in addition to scattering, strong atmospheric absorption leads to significant signal attenuation and so limits achievable rates.

These properties have motivated development of UV signal propagation models and communication systems for military and civilian applications, for example, long-range communication based on high-power UV lasers since the 1960s [5–8]. Recent progress in deep UV light emitting diodes (LEDs) [9] and avalanche photo-diodes (APDs) [10, 11] offers promise for deployment of low-cost/power and moderate bandwidth short-range UV communication systems [12, 13], including underwater communications [14, 15] and sensor networks [16, 17].

NLOS channel modeling is more complex than traditional LOS links. In addition to wavelength and device characteristics, NLOS path loss is a function of system geometry, including transmitter (Tx) beamwidth, communication range, receiver (Rx) FOV, the pointing elevation angles, as well as the optical properties of the atmosphere.

For simplicity and tractable analysis, single scattering models for NLOS communication links were developed [1, 18], with a corresponding single scattering assumption imposed; that is, each photon undergoes only a single interaction with the atmosphere before it reaches the detector. Recently the model has been further simplified for improved analytical tractability [19]. However, the single scattering assumption does not always lead to accurate link performance prediction, especially as the range increases, and with beam pointing at low elevation angles. Multiple scattering may occur when the particle density is large and/or

# Report Documentation Page

*Form Approved*
*OMB No. 0704-0188*

| 1. REPORT DATE **2010** | 2. REPORT TYPE | 3. DATES COVERED **00-00-2010 to 00-00-2010** |
|---|---|---|

| 4. TITLE AND SUBTITLE **A Path LossModel for Non-Line-of-Sight Ultraviolet Multiple Scattering Channels** | 5a. CONTRACT NUMBER |
|---|---|
| | 5b. GRANT NUMBER |
| | 5c. PROGRAM ELEMENT NUMBER |
| 6. AUTHOR(S) | 5d. PROJECT NUMBER |
| | 5e. TASK NUMBER |
| | 5f. WORK UNIT NUMBER |
| 7. PERFORMING ORGANIZATION NAME(S) AND ADDRESS(ES) **Department of Electrical Engineering,University of California,Riverside,CA,92521** | 8. PERFORMING ORGANIZATION REPORT NUMBER |
| 9. SPONSORING/MONITORING AGENCY NAME(S) AND ADDRESS(ES) | 10. SPONSOR/MONITOR'S ACRONYM(S) |
| | 11. SPONSOR/MONITOR'S REPORT NUMBER(S) |

12. DISTRIBUTION/AVAILABILITY STATEMENT
**Approved for public release; distribution unlimited**

13. SUPPLEMENTARY NOTES

14. ABSTRACT

15. SUBJECT TERMS

| 16. SECURITY CLASSIFICATION OF: | | | 17. LIMITATION OF ABSTRACT | 18. NUMBER OF PAGES | 19a. NAME OF RESPONSIBLE PERSON |
|---|---|---|---|---|---|
| a. REPORT **unclassified** | b. ABSTRACT **unclassified** | c. THIS PAGE **unclassified** | **Same as Report (SAR)** | **13** | |

**Standard Form 298 (Rev. 8-98)**
Prescribed by ANSI Std Z39-18

the propagation distance is long. Alternatives to the single scattering model include an empirical path loss model [20] and a Monte Carlo statistical path loss model [2]. Those models are applicable for predicting path loss in a variety of scenarios and are generally more accurate than the single scattering model.

In this paper, following the same physical scattering law as the Monte Carlo statistical method [2, 21], we develop a stochastic analytical NLOS UV channel path loss model. We apply a stochastic analytical technique [22, 23] to theoretically derive the $n$th scattered signal energy collected by the detector. The model assumes that the photons are stochastically scattered and/or absorbed by the atmospheric particles and involves probabilistic modeling of photon random moving direction, distance, energy loss, and receiver capture after a specified number of scatterings. In order to obtain the $n$th-order scattered signal at the receiver, we trace the migration routes of a single photon through the medium. Its scattering distance and scattering angles follow certain probability distribution functions (PDFs) [24]. The propagation of a photon between two consecutive scatterers is modeled as a single scattering event. The probability of the photon arriving at the receiver is a function of the $n$ scattering events encountered. A similar technique has been applied to model multiply scattered lidar returns in cloudy media where significant scattering occurs [22]. To account for a divergent UV beam profile, the contributions of photons at all possible directions within the beam are integrated [25].

We assume a homogeneous atmosphere with constant scattering and absorption coefficients and ignore atmospheric turbulence. This assumes that different types of particles are well mixed and the environment is stationary. Photons are scattered elastically which conserves energy but incurs energy loss during propagation. The detector is assumed small in size compared with the propagation space and is regarded as a point detector with finite FOV.

Our model offers an analytical formulation for NLOS scattering channel path loss and provides a reference to easily check other models in a variety of system parameter settings. We consider the effects of different optical pointing geometries and find that path loss is relatively insensitive to the Tx beam angle but increases considerably with increased Tx/Rx elevation angles and decreased Rx FOV for medium communication range. Not surprisingly, numerical tests demonstrate good agreement with Monte Carlo simulation [2]. However, the current analytical approach can distinguish the contributions of different orders of multiple scattering, whereas Monte Carlo modeling can only capture the total scattering effect. A similar comparison of Monte Carlo simulation and analytical methods has also been described by Lavigne et al. [26].

The model reveals when high-order scattering plays a role, and thus offers more insight into the channel behavior. Extensive numerical tests show that high-order scattering may play a significant role for scenarios with large baseline ranges and elevation angles. Atmospheric conditions also affect the multiple scattering contributions. A tenuous atmosphere generally leads to higher path loss at
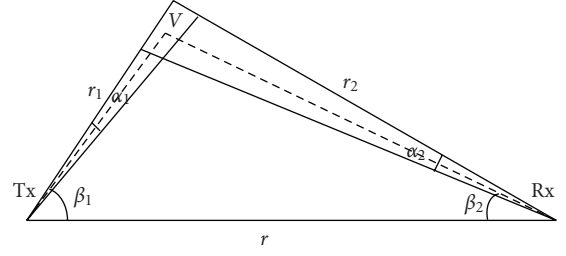
a small range than a thick or extra thick atmosphere where rich multiple scattering enhances received signal strength. As a by-product, when contributions from only single scattering are retained, the corresponding single scattering path loss shows a good match with that predicted by Reilly's analytical single scattering model [1]. A disadvantage of the proposed model is that it cannot provide pulse spreading information, while the Monte Carlo model can [2].

The organization of this paper is as follows. The stochastic path loss model based on a general NLOS UV channel configuration is developed in Section 2. It consists of modeling photon direction, distance traveled, probability of arrival at the receiver after scattering $n$ times, and total path loss. Numerical analysis for the multiple scattering NLOS channel is carried out and path loss performance is compared with both the single scattering model and Monte Carlo simulation in Section 3. Channel characteristics under different geometric parameters are analyzed in Section 4. Finally some conclusions are drawn.

## 2. Stochastic Path Loss Model

A NLOS UV channel involves rich scattering and absorption because of abundant suspended particulates in the atmosphere. For NLOS UV communication, scattering serves as the vehicle for information exchange between the Tx and Rx. The scattered photons that reach the receiver depend on the link geometry, the atmospheric optical properties, and their random migration, as described next.

*2.1. Link Geometry.* Consider a typical NLOS communication geometry [19, 20], as shown in Figure 1. Denote the Tx beam full-width divergence by $\alpha_1$, the Rx FOV angle by $\alpha_2$, the Tx elevation angle by $\beta_1$, Rx elevation angle by $\beta_2$, the Tx and Rx baseline separation by $r$, and the distances of the intersected (overlap) volume $V$ to the Tx and Rx by $r_1$ and $r_2$, respectively.

*2.2. Atmospheric Optical Properties.* From the communications viewpoint, scattering and absorption are two dominant types of photon interactions with the atmosphere. To describe a homogeneous atmospheric medium related to UV communication, we adopt the following coefficients [1, 26]:



FIGURE 1: NLOS UV communication link geometry, depicting elevated transmitter beam and receiver field-of-view.

the Rayleigh (molecular) scattering coefficient $k_s^{\text{Ray}}$, Mie (aerosol) scattering coefficient $k_s^{\text{Mie}}$, absorption coefficient $k_a$, and extinction coefficient $k_e$. The total scattering coefficient is defined as the sum of the two scattering coefficients $k_s = k_s^{\text{Ray}} + k_s^{\text{Mie}}$, and the extinction coefficient is given by the sum of the scattering and absorption coefficients as $k_e = k_s + k_a$.

The scattering phase function is modeled as a combined function of Rayleigh and Mie scattering phase functions based on the corresponding scattering coefficients [19, 27]:

$$P(\mu) = \frac{k_s^{\text{Ray}}}{k_s} p^{\text{Ray}}(\mu) + \frac{k_s^{\text{Mie}}}{k_s} p^{\text{Mie}}(\mu), \qquad (1)$$

where $\mu = \cos\theta$ is defined from the scattering angle $\theta$. The two-phase functions follow a generalized Rayleigh model and a generalized Henyey-Greenstein function, respectively:

$$p^{\text{Ray}}(\mu) = \frac{3[1 + 3\gamma + (1 - \gamma)\mu^2]}{16\pi(1 + 2\gamma)}, \qquad (2)$$

$$p^{\text{Mie}}(\mu) = \frac{1 - g^2}{4\pi}\left[\frac{1}{(1 + g^2 - 2g\mu)^{3/2}} + f\frac{0.5(3\mu^2 - 1)}{(1 + g^2)^{3/2}}\right], \qquad (3)$$

where $\gamma$, $g$, and $f$ are relevant model parameters.

*2.3. Elementary Events for Photon Random Migration.* Generally, it is impossible to predict with certainty the trajectory of a photon that travels in a medium of randomly distributed scattering and absorption particles. However, based on single scattering theory, we can obtain the probabilities for a photon's trajectory and calculate its multiple scattering arrival probability at the detector. The photon's trajectory can be exactly described by scattering distance, scattering zenith angle $\theta$, and scattering azimuth angle $\phi$. We first present the PDFs of these three fundamental elements for our modeling. The distance between neighboring scatters can be modeled from sampling a uniform random variable $x$ between zero and one as $r = -\ln x/k_s$ [28]. Accordingly after density transformation [29], the PDF of the scattering distance $r$ becomes

$$f_r(r) = k_s e^{-k_s r}. \qquad (4)$$

The sample space for variable $r$ is $[0, \infty]$. The PDFs for zenith scattering angle $\theta$ and azimuth angle $\phi$ can be further formulated based on the scattering phase function. The zenith scattering angle under Rayleigh scattering, Mie

scattering, and combined Rayleigh and Mie scattering has the following PDFs:

$$f_\theta^{\text{Ray}}(\theta) = \frac{3[1 + 3\gamma + (1 - \gamma)\cos^2\theta]}{8(1 + 2\gamma)}, \qquad (5)$$

$$f_\theta^{\text{Mie}}(\theta) = \frac{1 - g^2}{2}\left[\frac{1}{(1 + g^2 - 2g\cos\theta)^{3/2}} + f\frac{0.5(3\cos^2\theta - 1)}{(1 + g^2)^{3/2}}\right], \qquad (6)$$

$$f_\theta(\theta) = \frac{k_s^{\text{Ray}}}{k_s} f_\theta^{\text{Ray}}(\theta) + \frac{k_s^{\text{Mie}}}{k_s} f_\theta^{\text{Mie}}(\theta), \qquad (7)$$

where $\theta$ takes values in $[0, \pi]$. We consider a uniform distribution between 0 and $2\pi$ for azimuth scattering angle $\phi$ because there is no azimuth dependence in the phase function (symmetry is assumed). Thus, the azimuth scattering angle assumes the following PDF:

$$f_\phi(\phi) = \frac{1}{2\pi}, \quad \phi \in [0, 2\pi]. \qquad (8)$$

*2.4. Modeling of n Times Scattering.* With those probabilities, we are able to develop a probability model for a photon to be received by the detector after exactly $n$ scatterings. Assume that a photon from a UV source is uniformly emitted within the beam divergence and centered at direction angles $\theta_0$ and $\phi_0$, and migrates a distance $r_0$ before the first scattering happens. The solid angle within the beam can thus be modeled as a uniform random variable with a constant PDF of $1/\Omega_s$ where $\Omega_s$ is the source beam solid angle as $\Omega_s = 2\pi(1 - \cos(\alpha_1/2))$. The probability that it is scattered in the infinitesimal solid angle $d\Omega_0 = \sin(\theta_0)d\theta_0 d\phi_0$ becomes $1/\Omega_s \sin(\theta_0)d\theta_0 d\phi_0$ [22], and the probability that it moves an incremental distance $dr_0$ with attenuation is $e^{-k_a r_0} f_{r_0}(r_0)dr_0$. Therefore the probability that this photon lies away from the scatter center by $r_0$ and further moves $dr_0$ along the infinitesimal solid angle is the product of these two probabilities:

$$dQ_0 = \frac{e^{-k_a r_0}}{\Omega_s} f_{r_0}(r_0) \sin(\theta_0)d\theta_0 d\phi_0 dr_0. \qquad (9)$$

Notice that we adopt $k_a$ for exponential absorption loss within distance $r_0$ while the scattering effect has been absorbed in the scattering distance PDF. After arriving at the first scattering center, the photon is scattered and then continues to move with attenuation. The scattering center is regarded as a secondary point source emitting photons spatially following the angle PDFs described by (7) and (8). From the $i$th scattering center to the $(i+1)$th scattering center $(i = 1, 2, \ldots)$, a similar small probability $dQ_i$ conditioned on
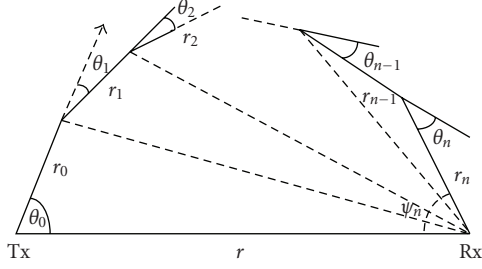
FIGURE 2: Photon migration path for $n$ scatterings.

all previous events can be written as

$$dQ_i = e^{-k_a r_i} f_{r_i}(r_i) f_{\theta_i}(\theta_i) f_{\phi_i}(\phi_i) \sin(\theta_i) d\theta_i d\phi_i dr_i. \quad (10)$$

The same procedure can be successively applied for each scattering process. Assume that each scattering is self-governed, and the distances and angles for different scattering events are conditioned on previous quantities. Therefore, the arrival probability for a photon that is scattered $n$ times before arriving at the Rx can be derived based on these transitions. Figure 2 shows the photon trajectory corresponding to $n$ scatterings.

After the $n$th scattering, we focus on an infinitesimal solid angle within the receiver FOV in order for the receiver to receive this photon. Define the direction angle $\psi_n$ as the angle between the line connecting the receiver and the $n$th scattering center and the transmitter-receiver separation line. Since the FOV has angle range of $[\beta_2 - \alpha_2/2, \beta_2 + \alpha_2/2]$ as shown in Figure 1, we can confine the photon direction using an indicator function $I_n$ which equals one when the condition $(\beta_2 - \alpha_2/2) < \psi_n < (\beta_2 + \alpha_2/2)$ is satisfied and zero otherwise. Therefore, the probability of the photon leaving the $n$th scattering center and reaching the detector becomes

$$dQ_n = I_n e^{-k_e r_n} f_{\theta_n}(\theta_n) f_{\phi_n}(\phi_n) \sin(\theta_n) d\theta_n d\phi_n. \quad (11)$$

We define the photon arrival probability after $n$ scatterings as $P_n$; that is, a photon undergoes $n$ scatterings and arrives at the Rx. The photon trajectory is uniquely described by $[(r_0, \ldots, r_n), (\theta_0, \ldots, \theta_n), (\phi_0, \ldots, \phi_n)]$, which are scattering distance set, scattering zenith angle set, and scattering azimuth angle set for $n$ successive scatterings, respectively. These variables are associated with each other using distance vectors $\vec{r}_i$ for $i = 0, \ldots, n$, and all involved distances and scattering angles can be recursively obtained from the previous distance vectors [2, 28]. Finally we obtain

$$P_n = \int \int \cdots \int dQ_0 \times dQ_1 \cdots \times dQ_n, \quad (12)$$

where $dQ_0$ is given by (9), $dQ_i$ by (10), and $dQ_n$ by (11). The integration limits for all variables cover their full ranges except the following: $\theta_0$ from $(\beta_1 - \alpha_1/2)$ to $(\beta_1 + \alpha_1/2)$ to ensure integration inside the source beam, and $\theta_n$ and $\phi_n$ within the solid angle of the receiver determined by the receiver area and distance $r_n$. Note that no integration over

$r_n$ is needed because it is a function of the other variables. Thus, there are a total of $3(n + 1) - 1$ integration variables.

In our model, the arrival probability $P_n$ is expressed through a multidimensional integral, and a closed form is not available. The dependence of $r_n$ and $I_n$ on other variables creates additional difficulty in model evaluation, and as $n$ increases, the complexity increases. Hence we apply a Monte Carlo integration technique, a powerful but simple numerical integration method for the approximate evaluation of definite integrals [30]. The idea is to generate a large number of random sample points uniformly distributed in the multidimensional hypercube $D$ and then calculate the average value of the integrand from the random samples [22, 30]. In our case we proceed as follows. There are $(n + 1)$ subspaces for $3(n + 1) - 1$ integrals, represented by all the $dQ_i$. We randomly generate sample points for the first $n$ subspace integrations, and calculate the corresponding integrands from the generated sample points $(r_i, \theta_i, \phi_i)$ $(i = 0, 1, \ldots, n - 1)$, denoted by vector $\vec{r}_i$. We then obtain the location of the $n$th scattering center and calculate the quantity $r_n$ from all those sample values. Applying these results, we further calculate the index function $I_n$. If it is one, then we randomly generate a sample point for $(\theta_n, \phi_n)$ and perform the integration over the detector area. This completes one sampling step. Suppose that the sample has a sufficiently large size $M$, and denote the points in the sample by $\vec{R}_1, \ldots, \vec{R}_M$. Then the estimate for the integral is given by

$$P_n = \int_D F(\vec{R}) d\vec{R} \approx \frac{D}{M} \sum_{i=1}^{M} F(\vec{R}_i), \quad (13)$$

where for notational convenience $F(\cdot)$ represents the integrand product of functions over all $dQ_i$, and $d\vec{R}$ for all differentials $d\vec{r}_i$. During the process, we truncate the infinite integration limit for all $r_i$ (up to $i = n - 1$) at a sufficiently large number to ensure that the integrand has decayed sufficiently close to zero. We have found generally that using a limit of several times $1/k_s$ works well.

It is important to clarify the difference between the *Monte Carlo integration* of a definite integral as used here and the *Monte Carlo simulation* of a stochastic process [2]. Even though both belong to the Monte Carlo family and involve random realizations, Monte Carlo integration is a numerical method based on the approximation of the averaged deterministic integrand function, whereas Monte Carlo simulation is a technique that relies on repeated samplings (numerous realizations) of a random process to compute a statistical expectation.

*2.5. Energy Loss Model.* To obtain the NLOS channel energy loss, we assume that a UV source emits a pulse containing $N$ photons uniformly within the beam angle $\alpha_1$, and each photon has an energy $\epsilon$. So the total transmitted energy is $E_t = \epsilon N$. The received energy after $n$ scatterings can be represented as
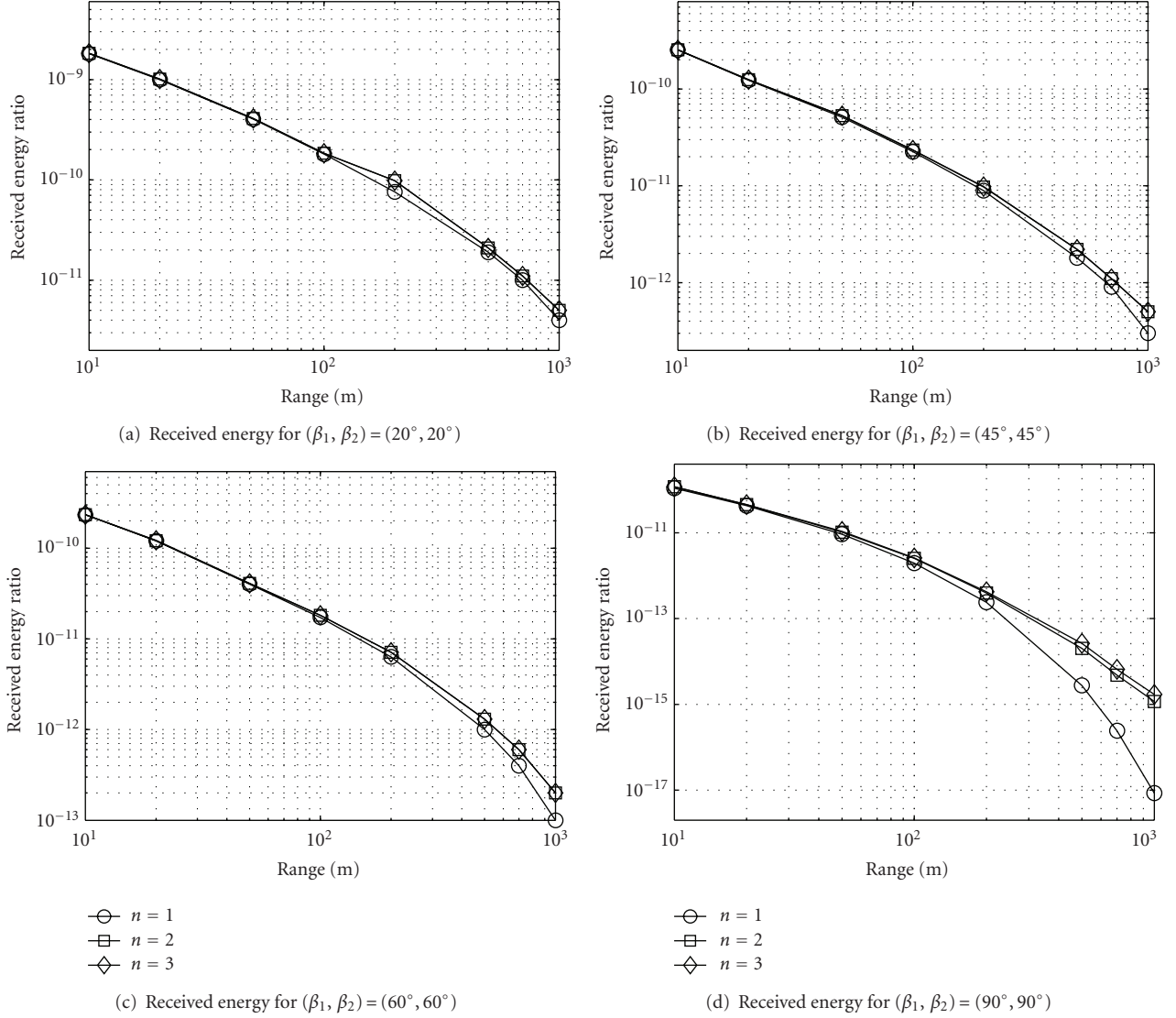
$$E_r(n) = E_t P_n. \quad (14)$$

(a) Received energy for $(\beta_1, \beta_2) = (20°, 20°)$

(b) Received energy for $(\beta_1, \beta_2) = (45°, 45°)$

$\begin{array}{l} \multimap\!\!\ominus\ \ n = 1 \\ \multimap\!\!\boxminus\ \ n = 2 \\ \multimap\!\!\diamondsuit\ \ n = 3 \end{array}$

(c) Received energy for $(\beta_1, \beta_2) = (60°, 60°)$

$\begin{array}{l} \multimap\!\!\ominus\ \ n = 1 \\ \multimap\!\!\boxminus\ \ n = 2 \\ \multimap\!\!\diamondsuit\ \ n = 3 \end{array}$

(d) Received energy for $(\beta_1, \beta_2) = (90°, 90°)$

FIGURE 3: Received energy ratio predicted by the proposed model.

The $n$th scattering path loss is modeled as

$$\mathrm{PL}(n) = \frac{E_t}{E_r(n)} = \frac{1}{P_n}. \qquad (15)$$

The received total energy up to $n$ scatterings is

$$E_{r,n} = \sum_{i=1}^{n} E_r(i) = E_t \sum_{i=1}^{n} P_i. \qquad (16)$$

From this result, the received energy ratio defined as $E_{r,n}/E_t$ becomes $\sum_{i=1}^{n} P_i$, and the corresponding path loss can be expressed as

$$\mathrm{PL}_n = \frac{E_t}{E_{r,n}} = \frac{1}{\sum_{i=1}^{n} P_i}. \qquad (17)$$

Note that when $n = \infty$, the energy represents the total received energy contributed by all scatterings and path loss represents the actual link performance. If we adopt decibels for path loss, then it becomes $10\log_{10}(\mathrm{PL}_n)$.

## 3. Modeling Performance

In this section we study modeling performance in terms of the received energy ratio and path loss results for different geometry scenarios. Through numerical simulation, multiple scattering effects are observed and analyzed. These results are also compared with Reilly's analytical single scattering model [1] as well as the Monte Carlo simulated multiple scattering model [2], respectively, under the same geometries and atmosphere parameters. We demonstrate good agreement with [1] when single scattering is of concern, and with [2] when multiple scatterings are considered.

(a) Path loss for $(\beta_1, \beta_2) = (20°, 20°)$

(b) Path loss for $(\beta_1, \beta_2) = (45°, 45°)$

(c) Path loss for $(\beta_1, \beta_2) = (60°, 60°)$

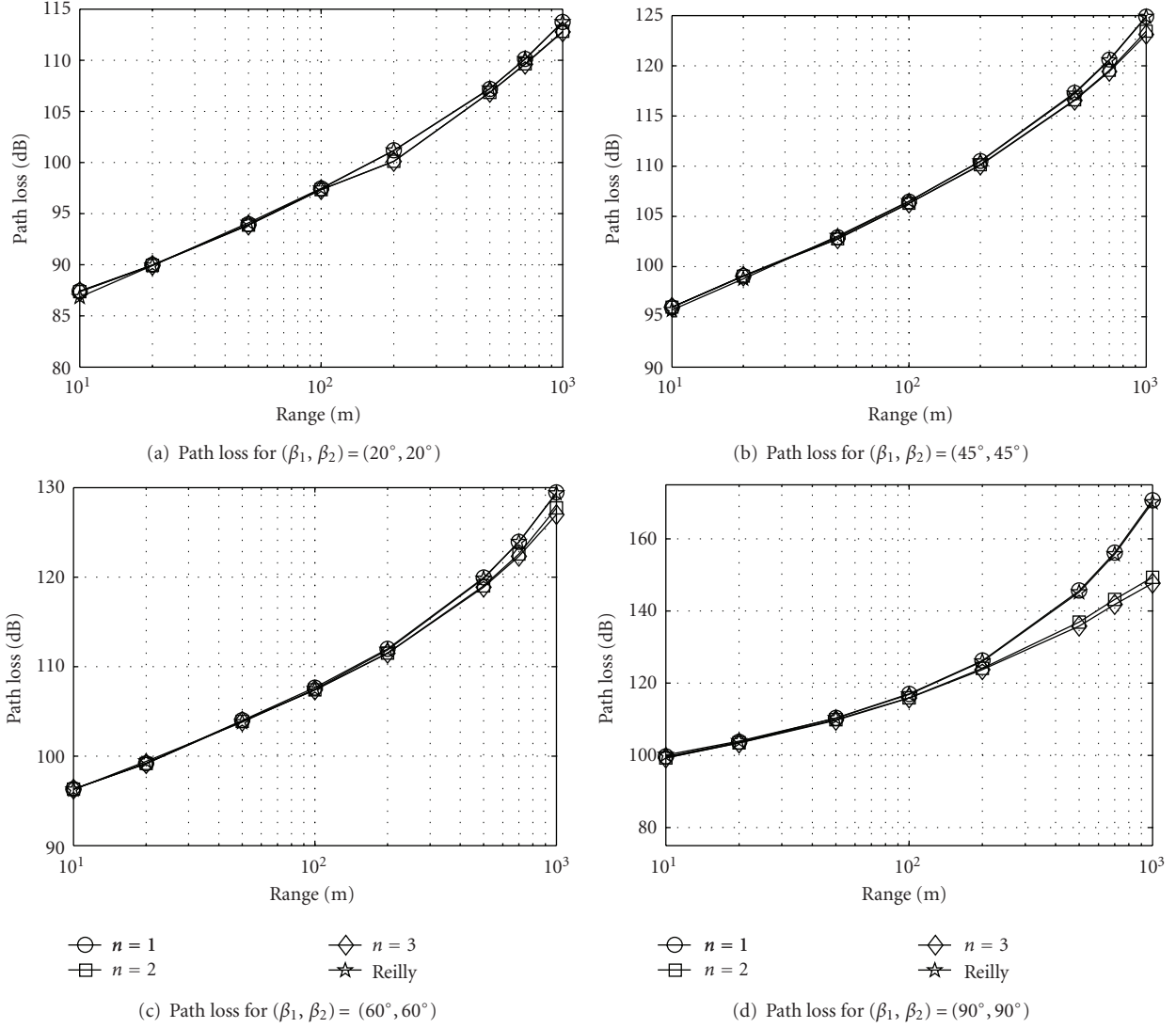(d) Path loss for $(\beta_1, \beta_2) = (90°, 90°)$

Figure 4: Path losses predicted by the proposed model and Reilly's model [1].

We assume gas concentrations and optical features of the atmosphere described by [7, Table II] for middle UV at wavelength 260 nm. Large dynamic ranges for the absorption and Mie scattering coefficients indicate that weather conditions may significantly affect the UV signal propagation. However, an explicit correspondence between the parameter settings and weather conditions is not available in the literature. Therefore we consider atmosphere coefficients for typical tenuous, thick, and extra thick atmosphere conditions (corresponding to clear, overcast, and foggy), given in Table 1. The tenuous condition will be adopted for all the following results unless stated otherwise. This agrees with the experimental measurement conditions in [13]. We set the geometric and model parameters as follows: $(\alpha_1, \alpha_2, \beta_1, \beta_2)$ = $(17°, 30°, 60°, 60°)$, $r$ ranges from 10 m to 1000 m, $\gamma$ = 0.017, $g$ = 0.72, $f$ = 0.5, and the detector area is 1.77 cm². Unless otherwise specified, the same parameters are used in Section 4.

To illustrate the importance of multiple scattering, consider the following example. Figure 3 shows the ratio of the accumulated received energy from $n = 1$ (1st scattering order only) to $n = 2$ (sum of 1st and 2nd-order scatterings), and $n = 3$ (sum of 1st, 2nd and 3rd order scatterings), all predicted via our proposed stochastic modeling for different optical geometries. We observe that, for each scenario, the 2nd-order scattering contributes little to the total received energy for ranges within 100 meters, but it will increasingly contribute more with longer ranges and larger pointing angles. Further, considering $n = 3$ does not add much to the received energy. For this case, 2nd-order scattering is sufficient because 3rd order scattering makes only a negligible contribution to the received energy.

The received signal energy can be transformed to the link path loss in decibels, depicted for different geometries in Figure 4. We also compare the proposed model with Reilly's

(a) Path loss for $(\beta_1, \beta_2) = (20°, 20°)$

(b) Path loss for $(\beta_1, \beta_2) = (45°, 45°)$

Stochastic
Simulation
(c) Path loss for $(\beta_1, \beta_2) = (60°, 60°)$

Stochastic
Simulation
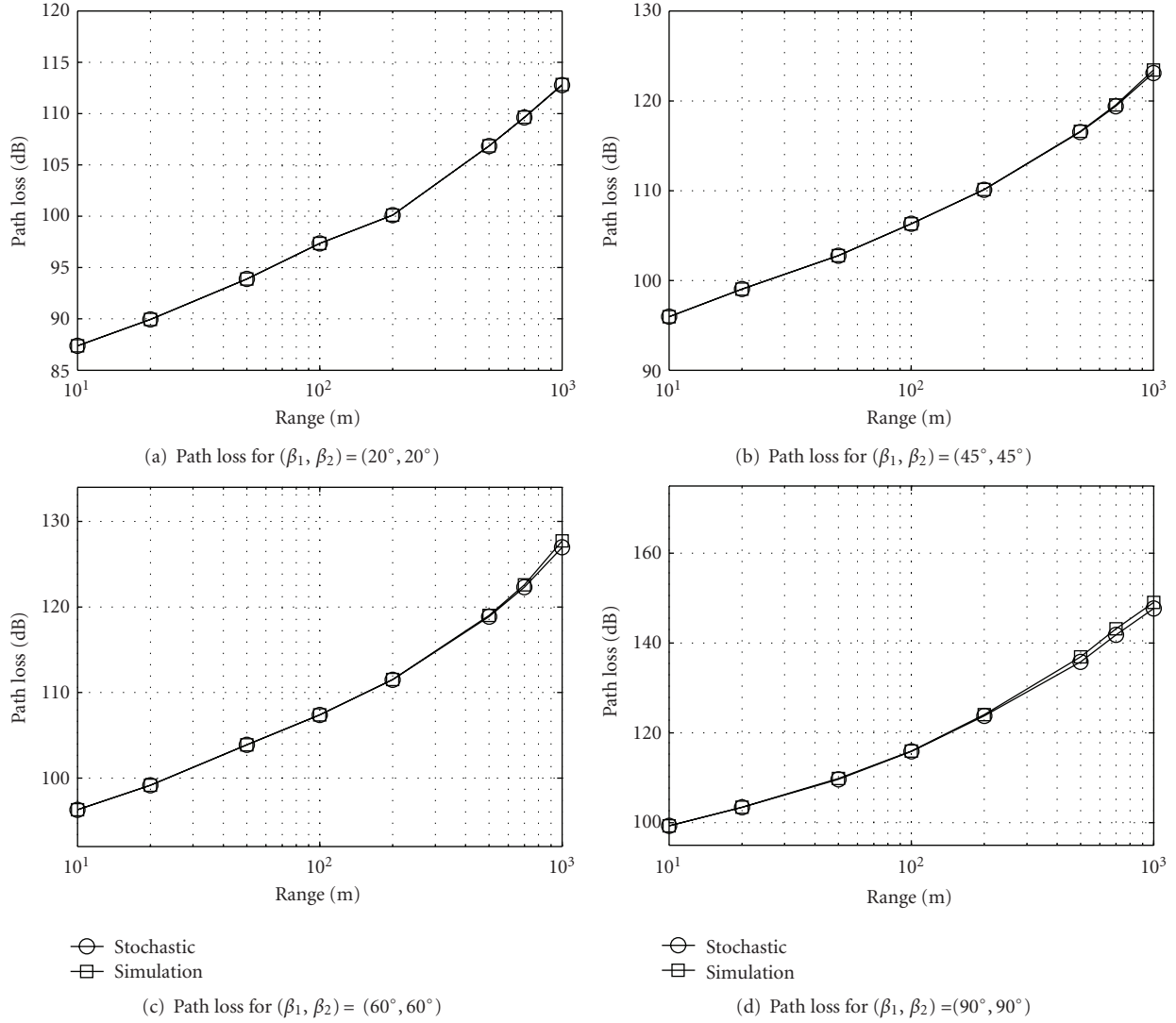(d) Path loss for $(\beta_1, \beta_2) = (90°, 90°)$

FIGURE 5: Comparison of the proposed stochastic model with the Monte Carlo simulation model [2].

single scattering model. Both models predict similar path loss levels for $n = 1$. As expected, including multiple scattering reduces predicted path loss. The improvement is not obvious for short range, consistent with Figure 3. Again, the 3rd-order scattering does not lead to a significant improvement for the received energy for these cases.

Due to the fact that our proposed stochastic model has the same premise that underlies the Monte Carlo simulation, we should expect the similar path loss from both models. As an example, Figure 5 compares the path loss results generated from our stochastic model and the Monte Carlo simulation model. Four sets of Tx and Rx elevation angles are included for detailed comparison. For each subplot, the stochastic model provides a good match with the simulation model within the high precision numerical accuracy of the simulation. This indicates that our proposed model is a good reference for evaluating the Monte Carlo simulation model.

## 4. NLOS UV Channel Characteristics

Since NLOS UV channel characteristics are crucial to communication system design, in this section, we apply the proposed multiple scattering model to further study the effects of different system parameters on the channel path loss, including link geometries and two typical atmosphere conditions. Referring to Figure 1, we study angle sensitivity by varying one angle and keeping the others fixed.

Figure 6 illustrates range-dependent path losses for (a) varying Tx elevation angle $\beta_1$, (b) varying Rx elevation angle $\beta_2$, (c) varying Tx beam angle $\alpha_1$, and (d) varying Rx FOV angle $\alpha_2$. Note that path loss is not very sensitive to the Tx beam angle. By contrast, path loss has the heaviest dependence on the Rx FOV angle. A wider FOV enables collection of more scattered photons which results in lower path loss. Path loss varies slightly with Rx elevation angle and moderately with Tx elevation angle. Larger baseline

(a) Path loss for different $\beta_1$

(b) Path loss for different $\beta_2$

(c) Path loss for different $\alpha_1$
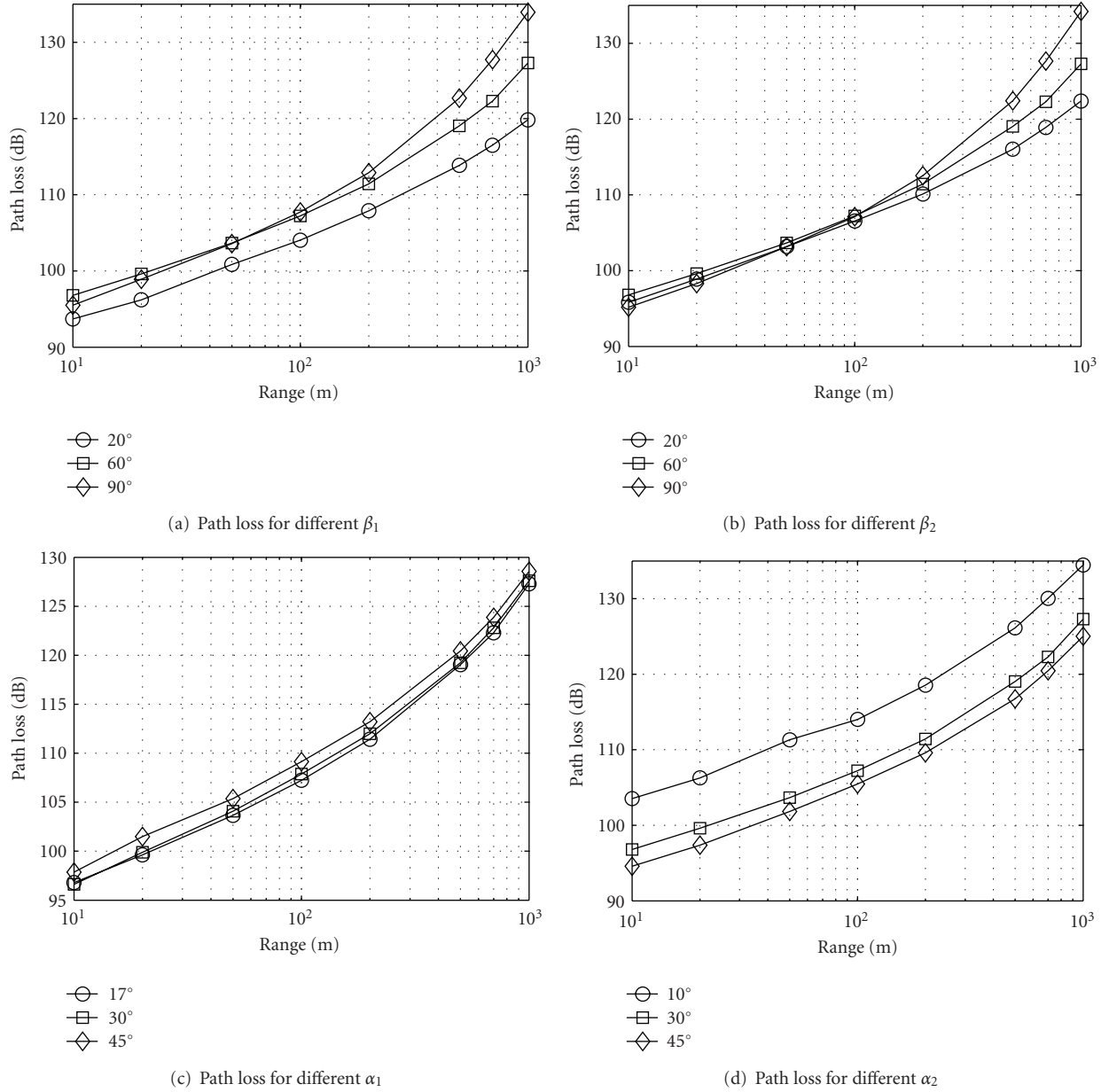
(d) Path loss for different $\alpha_2$

FIGURE 6: Predicted path loss for different system geometries.

range tends to make the angle effects more pronounced. As an example, in the first subplot for baseline range 1000 m, path losses for three different Tx elevation angles show differences up to 8 dB, while for a shorter range of 100 m, the difference is within 3 dB. Similar effects are obtained for other angular variation. One possible reason is that the roles of scattering and absorption may vary for different geometries. Larger propagation distance may bring about more scattered photons to the receiver but will also lead to higher absorption loss.

Up to now we have only considered tenuous atmospheric conditions. Next we consider the impact of atmospheric conditions on path loss. Figure 7 depicts range-dependent path loss for tenuous, thick, and extra thick atmosphere

conditions whose coefficients are given in Table 1. Four pairs of Tx and Rx elevation angles $(\beta_1, \beta_2)$ are incorporated for performance analysis. For elevation angle pair $(20°, 20°)$, path loss results for extra thick atmosphere are about 15 dB less than for tenuous, and 7 dB smaller than thick atmosphere at 10 m. As the range increases, path loss increases more dramatically. The gaps between curves decrease until a few hundred meters. Further range increase leads to a dramatic path loss increase for extra thick atmosphere. As elevation angles increase, the lower path loss region tends to shift to a smaller range. For example, for the medium elevation angle pairs $(45°, 45°)$ and $(60°, 60°)$, the lower attenuation range shrinks to less than 100 m, and for elevation angle pair $(90°, 90°)$, it reduces to less than 50 m.

(a) Path loss for $(\beta_1, \beta_2) = (20°, 20°)$

(b) Path loss for $(\beta_1, \beta_2) = (45°, 45°)$

- ⊖ Tenuous
- ⊟ Thick
- ⬦ Extra thick

(c) Path loss for $(\beta_1, \beta_2) = (60°, 60°)$

- ⊖ Tenuous
- ⊟ Thick
- ⬦ Extra thick

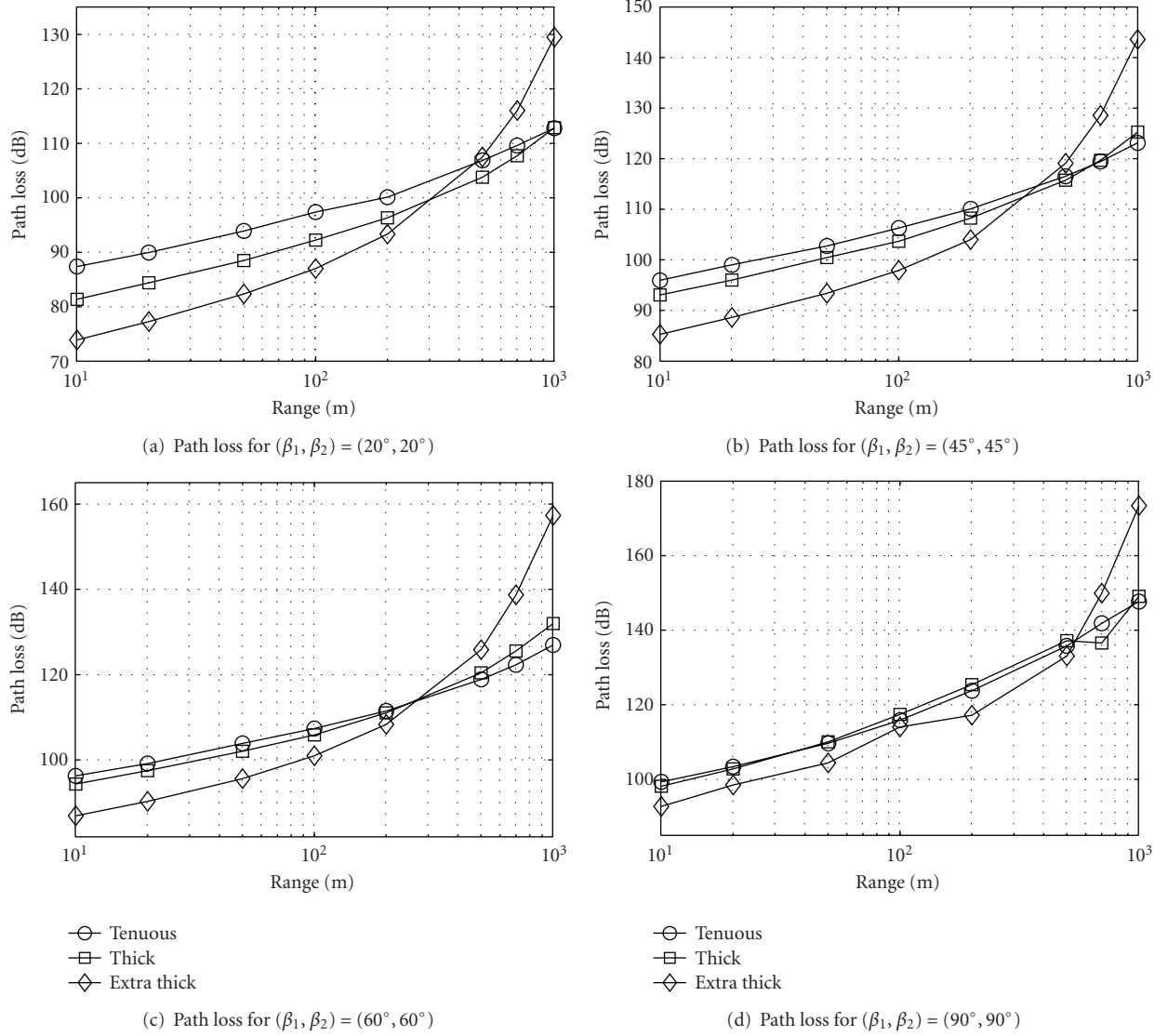(d) Path loss for $(\beta_1, \beta_2) = (90°, 90°)$

FIGURE 7: Predicted path loss for different atmosphere conditions.

TABLE 1: Atmosphere model parameters.

| Atmosphere | $k_s^{\text{Ray}}(\text{km}^{-1})$ | $k_s^{\text{Mie}}(\text{km}^{-1})$ | $k_a(\text{km}^{-1})$ |
|---|---|---|---|
| Tenuous | 0.266 | 0.284 | 0.972 |
| Thick | 0.292 | 1.431 | 1.531 |
| Extra thick | 1.912 | 7.648 | 1.684 |

In these scenarios, the scattering contribution dominates absorption loss for short ranges. For larger baseline ranges, scattering loss increases as the atmosphere gradually becomes thick and thus causes large path loss. For a given atmospheric condition, path loss increases by 20 dB to 40 dB when the elevation angle increases from 20° to 90° at short range. These observations and predictions are helpful for experimental channel characterization and communication system design.

In order to further demonstrate the significance of high-order scatterings, in Figure 8 we plot the ratio of the accumulated received energy from $n = 1$ (1st-order scattering only) to $n = 5$ (sum of 1st through 5th-order scatterings) for an extra thick atmosphere at different elevation angle pairs. For each pointing scenario, we observe that the 1st-order scattering contributes dominantly to the total received energy for short ranges up to 20 m. As the range increases, high-order scattering will contribute more to the total received energy. For example, the 2nd-, 3rd-, and 4th-order scattering overwhelm other order scattering for elevation angle (90°, 90°) at a range of 1000 m. Further, we can see that the 5th-order scattering does not contribute as much as the lower order scatterings. We also depict the corresponding path loss in Figure 9. When considering multiple scattering contributions, the path loss decreases as higher order scattering contributions are added. When compared with tenuous atmosphere, an extra thick atmosphere

(a) Received energy for $(\beta_1, \beta_2) = (20°, 20°)$

(b) Received energy for $(\beta_1, \beta_2) = (45°, 45°)$

(c) Received energy for $(\beta_1, \beta_2) = (60°, 60°)$

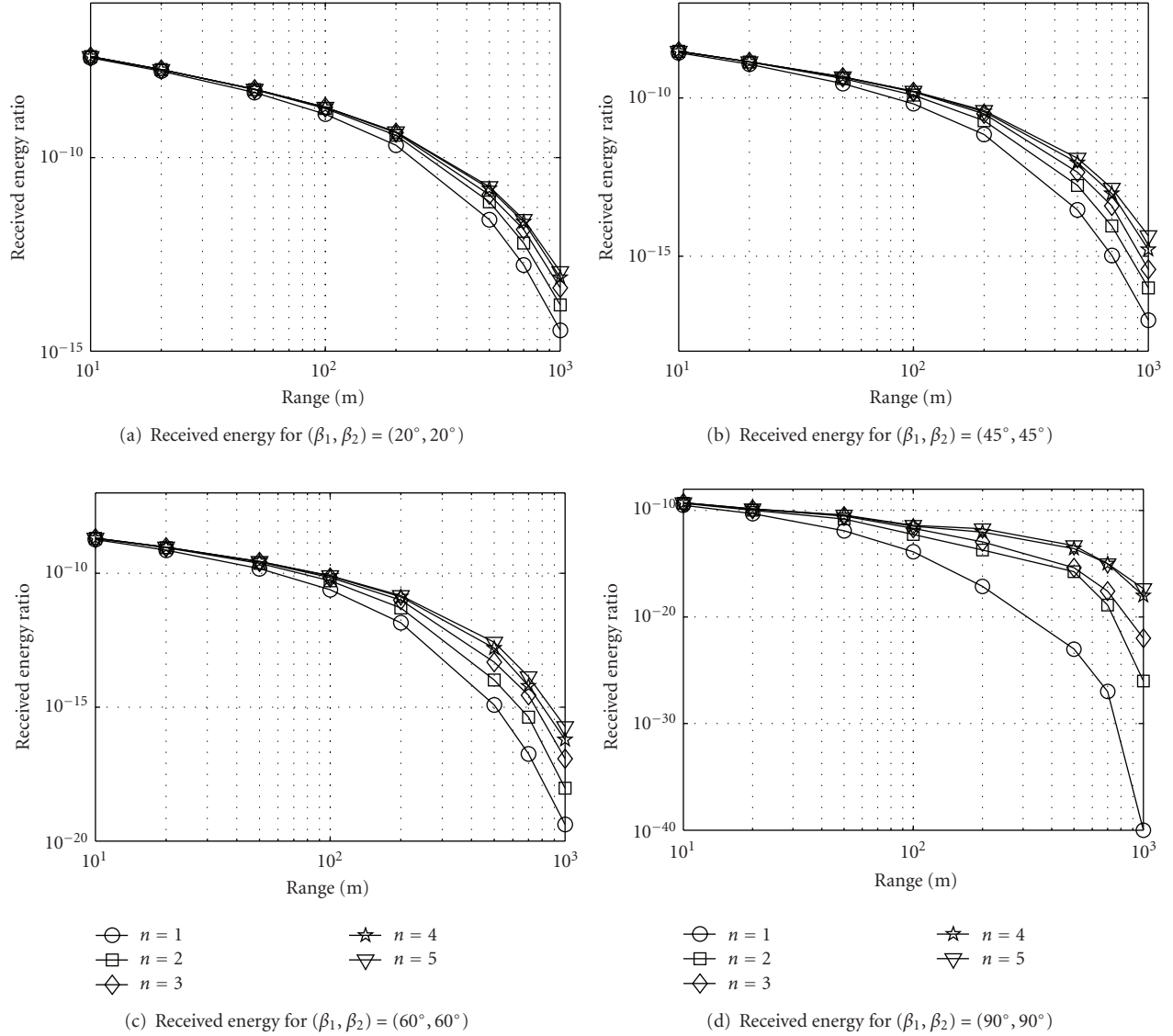(d) Received energy for $(\beta_1, \beta_2) = (90°, 90°)$

FIGURE 8: Received energy ratio for extra thick atmosphere predicted by the proposed model.

yields significant high-order scattering contributions, such as 3rd- and 4th-order scatterings, which should be accounted for when predicting path loss. These results indicate the remarkable property that for relatively shorter ranges, NLOS UV communications links are enhanced in hazy or foggy weather.

## 5. Conclusions

This paper proposed an analytical energy loss model for NLOS UV communication channels based on the probability theory of scattering and absorption. The model was developed by employing the PDFs of scattering distance and scattering angles. Multiple scattering was incorporated and contributions of different scattering orders were identified. The total energy loss was modeled by summing over the scattering order. The path loss predicted using only the contribution from the first-order agreed with Reilly's analytical single scattering model, as illustrated with different optical geometries. Multiple scattering becomes more dominant for some cases, especially longer propagation distance and larger elevation angles. Our model also provided results that are consistent with the Monte Carlo simulation model. Channel characteristics were investigated in detail, including the effects of varying system geometry and the effects of different atmosphere conditions.

Further study will be conducted to develop an analytical NLOS UV channel impulse response model from which our path loss model can be further validated and channel bandwidth can be predicted. An analytically more tractable path loss model is also a future topic of interest, which can enable more intuitive analysis for the effects of system geometry and parameters.
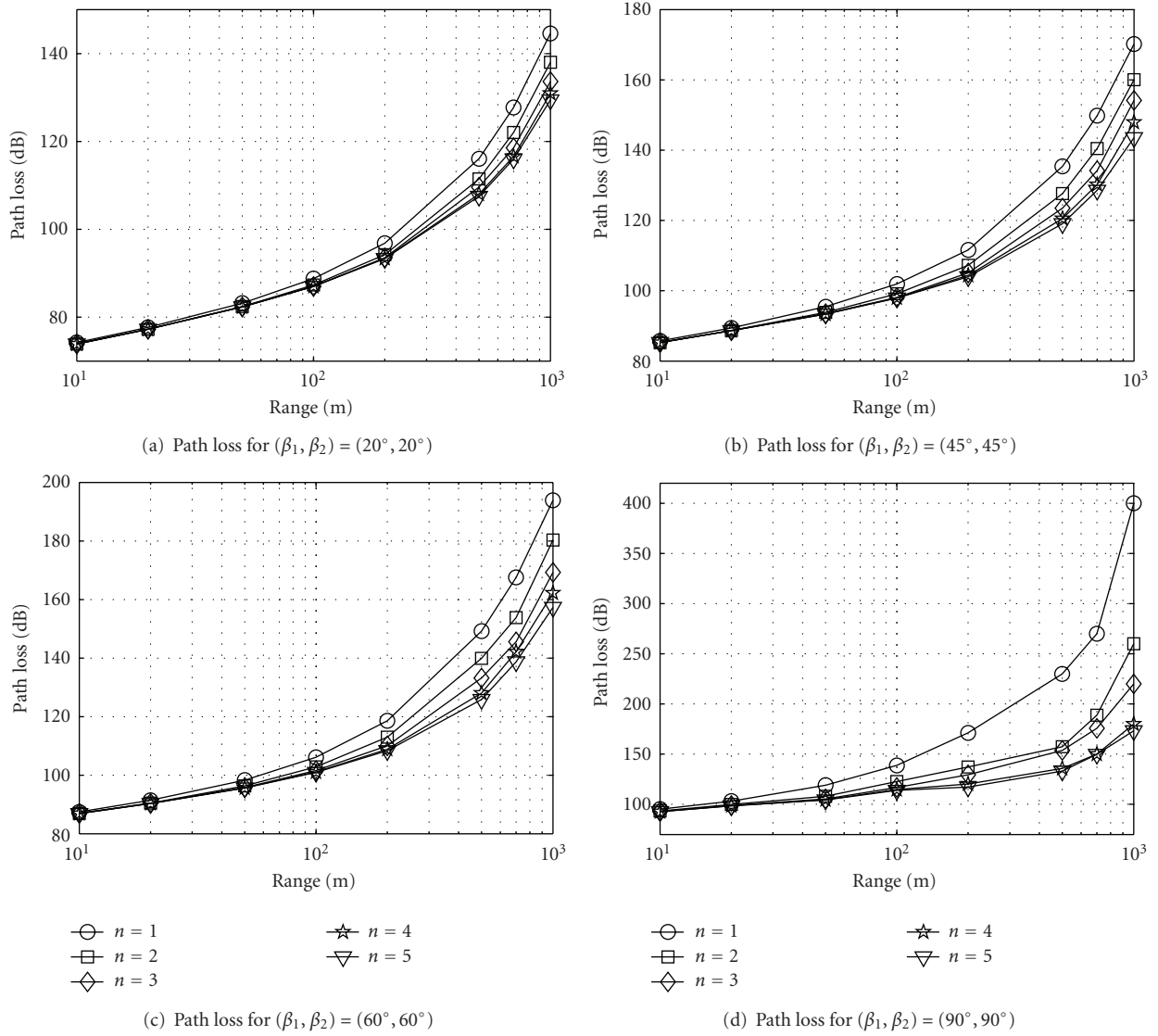
(a) Path loss for $(\beta_1, \beta_2) = (20°, 20°)$

(b) Path loss for $(\beta_1, \beta_2) = (45°, 45°)$

(c) Path loss for $(\beta_1, \beta_2) = (60°, 60°)$

(d) Path loss for $(\beta_1, \beta_2) = (90°, 90°)$

FIGURE 9: Predicted path loss for extra thick atmosphere.

## Acknowledgments

## References

[1] D. M. Reilly and C. Warde, "Temporal characteristics of single-scatter radiation," *Journal of the Optical Society of America A*, vol. 69, no. 3, pp. 464–470, 1979.

[2] H. Ding, G. Chen, A. K. Majumdar, B. M. Sadler, and Z. Xu, "Modeling of non-line-of-sight ultraviolet scattering channels for communication," *IEEE Journal on Selected Areas in Communications*, vol. 27, no. 9, pp. 1535–1544, 2009.

[3] Z. Xu and B. M. Sadler, "Ultraviolet communications: potential and state-of-the-art," *IEEE Communications Magazine*, vol. 46, no. 5, pp. 67–73, 2008.

[4] L. R. Koller, *Ultraviolet Radiation*, John Wiley & Sons, New York, NY, USA, 2nd edition, 1965.

[5] G. L. Harvey, "A survey of ultraviolet communication systems," Tech. Rep., Naval Research Laboratory, Washington, DC, USA, March 1964.

[6] D. E. Sunstein, *A scatter communication link at ultraviolet frequencies*, B.S. thesis, MIT, Cambridge, Mass, USA, 1968.

[7] D. M. Junge, *Non-line-of-sight electro-optic laser communications in the middle ultraviolet*, M.S. thesis, Naval Postgraduate School, Monterey, Calif, USA, December 1977.

[8] W. S. Ross and R. S. Kennedy, "An investigation of atmospheric optically scattered non-line-of-sight communication link," type, Army Research Office Project Report, Research Triangle Park, NC, USA, January 1980.

[9] M. Shatalov, J. Zhang, A. S. Chitnis, et al., "Deep ultraviolet light-emitting diodes using quaternary AlInGaN multiple

quantum wells," *IEEE Journal on Selected Topics in Quantum Electronics*, vol. 8, no. 2, pp. 302–309, 2002.

[10] X. Bai, D. Mcintosh, H. Liu, and J. C. Campbell, "Ultraviolet single photon detection with Geiger-mode 4H-SiC avalanche photodiodes," *IEEE Photonics Technology Letters*, vol. 19, no. 22, pp. 1822–1824, 2007.

[11] S. C. Shen, Y. Zhang, D. Yoo, et al., "Performance of deep ultraviolet GaN avalanche photodiodes grown by MOCVD," *IEEE Photonics Technology Letters*, vol. 19, no. 21, pp. 1744–1746, 2007.

[12] G. A. Shaw, A. M. Siegel, J. Model, and D. Greisokh, "Recent progress in short-range ultraviolet communication," in *Unattended Ground Sensor Technologies and Applications VII*, Proceedings of SPIE, pp. 214–225, Orlando, Fla, USA, March 2005.

[13] G. Chen, F. Abou-Galala, Z. Xu, and B. M. Sadler, "Experimental evaluation of LED-based solar blind NLOS communication links," *Optics Express*, vol. 16, no. 19, pp. 15059–15068, 2008.

[14] S. Arnon and D. Kedar, "Non-line-of-sight underwater optical wireless communication network," *Journal of the Optical Society of America A*, vol. 26, no. 3, pp. 530–539, 2009.

[15] D. Kedard and S. Arnon, "Subsea ultraviolet solar-blind broadband free-space optics communication," *Optical Engineering*, vol. 48, no. 4, Article ID 046001, 7 pages, 2009.

[16] G. A. Shaw, A. M. Siegel, J. Model, and M. Nischan, "Field testing and evaluation of a solar-blind UV communication link for unattended ground sensors," in *Unattended/Unmanned Ground, Ocean, and Air Sensor Technologies and Applications VI*, vol. 5417 of *Proceedings of SPIE*, pp. 250–261, Orlando, Fla, USA, April 2004.

[17] D. Kedar and S. Arnon, "Non-line-of-sight optical wireless sensor network operating in multiscattering channel," *Applied Optics*, vol. 45, no. 33, pp. 8454–8461, 2006.

[18] M. R. Luettgen, J. H. Shapiro, and D. M. Reilly, "Non-line-of-sight single-scatter propagation model," *Journal of the Optical Society of America A*, vol. 8, no. 12, pp. 1964–1972, 1991.

[19] Z. Xu, H. Ding, B. M. Sadler, and G. Chen, "Analytical performance study of solar blind non-line-of-sight ultraviolet short-range communication links," *Optics Letters*, vol. 33, no. 16, pp. 1860–1862, 2008.

[20] G. Chen, Z. Xu, H. Ding, and B. M. Sadler, "Path loss modeling and performance trade-off study for short-range non-line-of-sight ultraviolet communications," *Optics Express*, vol. 17, no. 5, pp. 3929–3940, 2009.

[21] A. N. Witt, "Multiple scattering in reflection nebulae—I: a Monte Carlo approach," *The Astrophysical Journal Supplement Series*, vol. 35, pp. 1–6, 1977.

[22] D. T. Gillespie, "Stochastic-analytic approach to the calculation of multiply scattered lidar returns," *Journal of the Optical Society of America A*, vol. 2, no. 8, pp. 1307–1324, 1985.

[23] D. T. Gillespie, "Calculation of *n*-scattered lidar retrens for large n in an idealized cloud," *Journal of the Optical Society of America A*, vol. 4, no. 3, pp. 455–464, 1987.

[24] A. H. Gandjbakhche, R. Nossal, and R. F. Bonner, "Scaling relationships for theories of anisotropic random walks applied to tissue optics," *Applied Optics*, vol. 32, no. 4, pp. 504–516, 1993.

[25] L. R. Bissonnette, "Multiple-scattering lidar equation," *Applied Optics*, vol. 35, no. 33, pp. 6449–6465, 1996.

[26] C. Lavigne, A. Roblin, V. Outters, S. Langlois, T. Girasole, and C. Rozé, "Comparison of iterative and Monte Carlo methods for calculation of the aureole about a point source in the Earth's atmosphere," *Applied Optics*, vol. 38, no. 30, pp. 6237–6246, 1999.

[27] A. S. Zachor, "Aureole radiance field about a source in a scattering-absorbing medium," *Applied Optics*, vol. 17, no. 12, pp. 1911–1922, 1978.

[28] S. A. Prahl, M. Keijzer, S. L. Jacques, and A. J. Welch, "A Monte Carlo model of light propagation in tissue," in *Dosimetry of Laser Radiation in Medicine and Biology*, vol. IS 5 of *Proceedings of SPIE*, pp. 102–111, 1989.

[29] A. Leon-Garcia, *Probability and Random Processes for Electrical Engineering*, Addison-Wesley, Reading, Mass, USA, 1994.

[30] Wikipedia, "Monte Carlo integration," http://en.wikipedia.org/wiki/Monte_Carlo_integration.

# EUSIPCO 2011
### 19th European Signal Processing Conference
### August 29- September 2, 2011, Barcelona (Spain)

Photograph © Turisme de Barcelona / J. Trullàs

## Preliminary call for papers

The 2011 European Signal Processing Conference (EUSIPCO-2011) is the nineteenth in a series of conferences promoted by the European Association for Signal Processing (EURASIP, www.eurasip.org). This year edition will take place in Barcelona, capital city of Catalonia (Spain), and will be jointly organized by the Centre Tecnològic de Telecomunicacions de Catalunya (CTTC) and the Universitat Politècnica de Catalunya (UPC).

EUSIPCO-2011 will focus on key aspects of signal processing theory and applications as listed below. Acceptance of submissions will be based on quality, relevance and originality. Accepted papers will be published in the EUSIPCO proceedings and presented during the conference. Paper submissions, proposals for tutorials and proposals for special sessions are invited in, but not limited to, the following areas of interest.

## Areas of Interest

- Audio and electro-acoustics.
- Design, implementation, and applications of signal processing systems.
- Multimedia signal processing and coding.
- Image and multidimensional signal processing.
- Signal detection and estimation.
- Sensor array and multi-channel signal processing.
- Sensor fusion in networked systems.
- Signal processing for communications.
- Medical imaging and image analysis.
- Non-stationary, non-linear and non-Gaussian signal processing.

## Submissions

Procedures to submit a paper and proposals for special sessions and tutorials will be detailed at www.eusipco2011.org. Submitted papers must be camera-ready, no more than 5 pages long, and conforming to the standard specified on the EUSIPCO 2011 web site. First authors who are registered students can participate in the best student paper competition.

## Important Deadlines:

| | |
|---|---|
| Proposals for special sessions | 15 Dec 2010 |
| Proposals for tutorials | 18 Feb 2011 |
| **Electronic submission of full papers** | **21 Feb 2011** |
| Notification of acceptance | 23 May 2011 |
| Submission of camera-ready papers | 6 Jun 2011 |

**Webpage: www.eusipco2011.org**

**Organizing Committee**

*Honorary Chair*
Miguel A. Lagunas (CTTC)

*General Chair*
Ana I. Pérez-Neira (UPC)

*General Vice-Chair*
Carles Antón-Haro (CTTC)

*Technical Program Chair*
Xavier Mestre (CTTC)

*Technical Program Co-Chairs*
Javier Hernando (UPC)
Montserrat Pardàs (UPC)

*Plenary Talks*
Ferran Marqués (UPC)
Yonina Eldar (Technion)

*Special Sessions*
Ignacio Santamaría (Unversidad de Cantabria)
Mats Bengtsson (KTH)

*Finances*
Montserrat Nájar (UPC)

*Tutorials*
Daniel P. Palomar
(Hong Kong UST)
Beatrice Pesquet-Popescu (ENST)

*Publicity*
Stephan Pfletschinger (CTTC)
Mònica Navarro (CTTC)

*Publications*
Antonio Pascual (UPC)
Carles Fernández (CTTC)

*Industrial Liaison & Exhibits*
Angeliki Alexiou
(University of Piraeus)
Albert Sitjà (CTTC)

*International Liaison*
Ju Liu (Shandong University-China)
Jinhong Yuan (UNSW-Australia)
Tamas Sziranyi (SZTAKI -Hungary)
Rich Stern (CMU-USA)
Ricardo L. de Queiroz  (UNB-Brazil)